

On the Influence of the Parameters of a Layered Target and an Electron Beam on Diffracted Transition Radiation and Parametric X-Rays

S. V. Blazhevich^a, O. Yu. Shevchuk^a, A. V. Noskov^{a, b, *}, and A. E. Fedoseev^a

^a Belgorod State National Research University, Belgorod, 308015 Russia

^b Shukhov Belgorod State Technological University, Belgorod, 308012 Russia

*e-mail: noskovbupk@mail.ru

Received July 21, 2022; revised September 30, 2022; accepted September 30, 2022

Abstract—The parametric X-rays and diffracted transition radiation of a beam of relativistic electrons crossing a target with a periodic layered structure in the Bragg scattering geometry are studied. The general case of asymmetric reflection of the electron field relative to the target surface is considered, i.e., the case when the target layers are located at an arbitrary angle to its surface. Expressions are obtained within the two-wave approximation of the dynamic theory of diffraction, which describe the angular densities of parametric X-rays and diffracted transition radiation and their interference. Numerical calculations of the angular densities of radiation are performed for various values of the target and electron-beam parameters. A dependence of the angular densities of parametric X-ray radiation and diffracted transition radiation on the divergence of the electron beam and relationship between the thicknesses of the periodic structure layers are demonstrated. With an increase in the electron energy, the dependence of the angular density of the diffracted transition radiation on the electron-beam divergence increases.

Keywords: electron-beam divergence, diffracted transition radiation, parametric X-ray radiation, relativistic electron

DOI: 10.1134/S1027451023030242

INTRODUCTION

The coherent X-ray radiation of a relativistic electron crossing a target, which is a periodic layered medium, was studied in [1] within the dynamic theory of diffraction. The radiation was considered as a result of the interference of parametric X-rays (PXR) and diffracted transition radiation (DTR). Parametric X-rays in a periodic layered medium arise due to the diffraction of pseudo-photons of the Coulomb field of a relativistic electron on target layers, similarly to how PXR occur in a single crystal due to diffraction at a system of parallel atomic planes [2, 3]. Diffracted transition radiation is a consequence of the diffraction of photons of transition radiation generated at the input surface of the target by its layers, in analogy with DTR in a single crystal [4–6]. The dynamic theory of the radiation of relativistic electrons in periodic layered media [1] describes well the published experimental data [7]. It should be noted that the radiation process in periodic layered media was traditionally considered in the Bragg scattering geometry and only for the particular case of the symmetric reflection of an electron field relative to the target surface when the angle between the target surface and the reflecting layers is equal to zero. Such a consideration was also used

in [1]. For the general case of asymmetric reflection of the electron field relative to the target surface, the process of the excitation of coherent X-ray radiation by a relativistic electron in a periodic layered medium was first considered in the Laue scattering geometry in [8] and in the Bragg scattering geometry in [9]. The authors of [10–20] developed a dynamic theory of coherent X-ray radiation excited by the transmission of a divergent beam of relativistic electrons through a target with a periodic layered structure and a single crystal.

In this study, the influence of the parameters of the target and the beam of relativistic electrons on the spectral angular characteristics of PXR and DTR is analyzed.

GEOMETRY OF THE RADIATION PROCESS

We consider a beam of relativistic electrons crossing a periodic structure in the Bragg scattering geometry (Fig. 1), a periodic layered target consisting of alternating layers with thicknesses of l_1 and l_2 ($T = l_1 + l_2$ is the period of the layered target), and with dielectric susceptibilities χ_1 and χ_2 , respectively. The layers

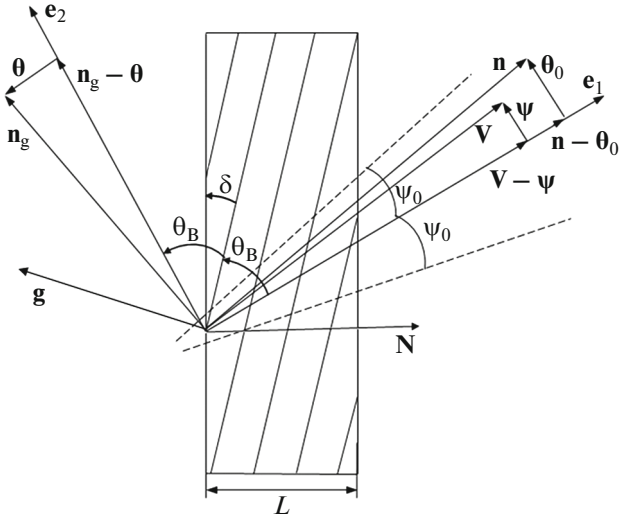


Fig. 1. Geometry of the radiation process.

reflecting radiation are located at some angle δ to the target surface (Fig. 1), which corresponds to the case of asymmetric reflection of the radiation field ($\delta = 0$ is a particular case of symmetric reflection). We introduce angular variables ψ , θ , and θ_0 in accordance with definitions of the relativistic electron velocity \mathbf{V} , unit vector \mathbf{n} in the direction of the momentum of a photon emitted near the direction of the electron-velocity vector, and unit vector \mathbf{n}_g in the direction of Bragg scattering, which are defined by the following formulas:

$$\begin{aligned} \mathbf{V} &= \left(1 - \frac{1}{2}\gamma^{-2} - \frac{1}{2}\psi^2\right)\mathbf{e}_1 + \boldsymbol{\psi}, \quad \mathbf{e}_1\boldsymbol{\psi} = 0, \\ \mathbf{n} &= \left(1 - \frac{1}{2}\theta_0^2\right)\mathbf{e}_1 + \boldsymbol{\theta}_0, \quad \mathbf{e}_1\boldsymbol{\theta}_0 = 0, \quad \mathbf{e}_1\mathbf{e}_2 = \cos 2\theta_B, \quad (1) \\ \mathbf{n}_g &= \left(1 - \frac{1}{2}\theta^2\right)\mathbf{e}_2 + \boldsymbol{\theta}, \quad \mathbf{e}_2\boldsymbol{\theta} = 0, \end{aligned}$$

where θ is the angle of radiation measured from the radiation-detector axis \mathbf{e}_2 , ψ is the angle of deviation of the considered electron in a beam measured from the electron-beam axis \mathbf{e}_1 , θ_0 is the angle between the direction of propagation of the incident photon and

the \mathbf{e}_1 axis, and $\gamma = 1/\sqrt{1-V^2}$ is the Lorentz factor of the electron. The angular variables are considered as the sum of the following components parallel and perpendicular to the plane of Fig. 1: $\boldsymbol{\theta} = \boldsymbol{\theta}_{\parallel} + \boldsymbol{\theta}_{\perp}$, $\boldsymbol{\theta}_0 = \boldsymbol{\theta}_{0\parallel} + \boldsymbol{\theta}_{0\perp}$, and $\boldsymbol{\psi} = \boldsymbol{\psi}_{\parallel} + \boldsymbol{\psi}_{\perp}$. The \mathbf{g} vector (Fig. 1) is similar to the reciprocal lattice vector in a crystal, i.e., it is perpendicular to the target layers and its length equals $g = \frac{2\pi}{T}n$, $n = 0, \pm 1, \pm 2, \dots$.

ANGULAR DENSITY OF RADIATION

In [10], a dynamic theory of coherent X-ray radiation excited by the transmission of a divergent beam of relativistic electrons through a periodic layered target was developed. In [10], the following expressions that describe the angular densities of PXR, DTR, and their interference in the case of a thin nonabsorbing target, for which the path length $L_f = L/\sin(\theta_B - \delta)$ of a diffracted photon in the target is much less than absorption length $L_{\text{abs}} = \frac{1+r}{\omega(\chi_1'' + r\chi_2'')}$ of X-ray waves in a periodic layered medium, were obtained:

$$\frac{dN_{\text{PXR}}^{(s)}}{d\Omega} = \frac{e^2\omega_B^3 T^2 L_{\text{ext}}^{(s)} \Omega^{(s)2}}{2\pi^4 n^2 \sigma^{(s)2}} \int_{\sqrt{\varepsilon}}^{\infty} R_{\text{PXR}}^{(s)} d\xi^{(s)}(\omega), \quad (2)$$

$$R_{\text{PXR}}^{(s)} = \frac{(\xi^{(s)} + \sqrt{\xi^{(s)2} - \varepsilon})^2 \sin^2\left(\frac{b^{(s)}}{2}\Sigma^+\right)}{\Sigma (\Sigma^+)^2}, \quad (3)$$

$$\begin{aligned} \frac{dN_{\text{DTR}}^{(s)}}{d\Omega} &= \frac{e^2\omega_B^3 T^2 L_{\text{ext}}^{(s)}}{2\pi^3 n^2} \\ &\times \frac{\Omega^{(s)2}}{\sigma^{(s)2}(\mathbf{v}^{(s)}\boldsymbol{\sigma}^{(s)} - 1)^2} \varepsilon\sqrt{\varepsilon} \tanh\left(\frac{b^{(s)}}{\sqrt{\varepsilon}}\right), \end{aligned} \quad (4)$$

$$\begin{aligned} \frac{dN_{\text{INT}}^{(s)}}{d\Omega} &= \frac{e^2\omega_B^3 T^2 L_{\text{ext}}^{(s)}}{2\pi^4 n^2} \\ &\times \frac{\Omega^{(s)2}}{\sigma^{(s)2}(\boldsymbol{\sigma}^{(s)}\mathbf{v}^{(s)} - 1)} \int_{\sqrt{\varepsilon}}^{\infty} R_{\text{INT}}^{(s)} d\xi^{(s)}(\omega), \end{aligned} \quad (5)$$

$$\begin{aligned} R_{\text{INT}}^{(s)} &= \frac{2\varepsilon^3}{\xi^{(s)2} - \varepsilon + \varepsilon \sin^2\left(\frac{b^{(s)}\sqrt{\xi^{(s)2} - \varepsilon}}{\varepsilon}\right)} \\ &\times \frac{\sigma^{(s)}\sqrt{\xi^{(s)2} - \varepsilon} \sin\left(\frac{b^{(s)}\sqrt{\xi^{(s)2} - \varepsilon}}{\varepsilon}\right) \sin\left(b^{(s)}\left(\frac{\xi^{(s)}}{\varepsilon} - \boldsymbol{\sigma}^{(s)}\right)\right) + (\boldsymbol{\sigma}^{(s)}\xi^{(s)} - 1) \sin^2\left(\frac{b^{(s)}\sqrt{\xi^{(s)2} - \varepsilon}}{\varepsilon}\right)}{(\xi^{(s)} - \varepsilon\boldsymbol{\sigma}^{(s)})^2 + \varepsilon - \xi^{(s)2}}, \end{aligned}$$

where

$$\begin{aligned}\Sigma &= \xi^{(s)2} - \varepsilon + \varepsilon \sin^2 \left(\frac{b^{(s)} \sqrt{\xi^{(s)2} - \varepsilon}}{\varepsilon} \right), \quad \Sigma^+ = \frac{\xi^{(s)} + \sqrt{\xi^{(s)2} - \varepsilon}}{\varepsilon} - \sigma^{(s)}, \\ \Omega^{(1)} &= \theta_{\perp} - \psi_{\perp}, \quad \Omega^{(2)} = \theta_{\parallel} + \psi_{\parallel}, \quad \sigma^{(s)} = \frac{\pi n}{C^{(s)} \left| \chi_2' - \chi_1' \right| \left| \sin \left(\frac{\pi n}{1+r} \right) \right|} \\ &\times \left(\gamma^{-2} + (\theta_{\perp} - \psi_{\perp})^2 + (\theta_{\parallel} + \psi_{\parallel})^2 - \chi_0' \right), \quad C^{(1)} = 1, \quad C^{(2)} = |\cos 2\theta_B|, \\ v^{(s)} &= \frac{C^{(s)} \left| \sin \left(\frac{\pi n}{1+r} \right) \right| \left| \chi_2' - \chi_1' \right|}{\frac{\pi n}{1+r} \left| \chi_1' + r\chi_2' \right|}, \quad b^{(s)} = \frac{1}{2 \sin(\theta_B + \delta)} \frac{L}{L_{\text{ext}}^{(s)}}, \\ \varepsilon &= \frac{\sin(\theta_B - \delta)}{\sin(\theta_B + \delta)}, \quad r = \frac{l_2}{l_1}, \quad \chi_0' = \frac{l_1 \chi_1' + l_2 \chi_2'}{T}, \\ L_{\text{ext}}^{(s)} &= \frac{1}{\omega \left| \sin \left(\frac{\pi n}{1+r} \right) \right| \left| \chi_2' - \chi_1' \right| C^{(s)}}, \quad \omega_B = \frac{\pi n}{T \sin \theta_B}, \\ \xi^{(s)}(\omega) &= \eta^{(s)}(\omega) + \frac{1 + \varepsilon}{2v^{(s)}}, \quad \eta^{(s)}(\omega) = \frac{2\pi^2 n^2}{T^2 \omega_B} L_{\text{ext}}^{(s)} \left(1 - \frac{\omega}{\omega_B} \left(1 - \theta_{\parallel} \sqrt{\frac{T^2 \omega_B^2}{\pi^2 n^2} - 1} \right) \right).\end{aligned}$$

Expressions (2)–(6) can be used to describe σ -polarized fields at the parameter value $s = 1$, and π -polarized fields at parameter value $s = 2$.

Since inequality $\frac{2\pi^2 n^2}{T^2 \omega_B} L_{\text{ext}}^{(s)} \gg 1$ is fulfilled in the range of X-ray frequencies, then $\eta^{(s)}(\omega)$ is a “fast” function of the frequency ω . Therefore, it is very convenient to consider $\eta^{(s)}(\omega)$ or $\xi^{(s)}(\omega)$ as a spectral variable that characterizes the frequency ω for further analysis of the PXR and DTR spectra.

Next, we average expressions (2) and (4) for the angular densities of the PXR and DTR of a single electron moving at an angle of $\psi(\psi_{\perp}, \psi_{\parallel})$ and expression (4) for their interference term over all possible rectilinear trajectories of this electron in the beam by using the following Gaussian distribution:

$$f(\psi) = \frac{1}{\pi \psi_0^2} \exp \left\{ -\frac{\psi^2}{\psi_0^2} \right\}, \quad (6)$$

where parameter ψ_0 will be called the divergence of the beam of emitting electrons in Fig. 1.

Angle ψ_0 is the dispersion of the distribution and determines a cone that limits a part of the electron beam, beyond which the electron density decreases by more than a factor of e with respect to the density on the beam axis. For this case, the expressions normalized to one electron, which describe the angular densities of PXR and DTR and their interference in the Bragg-scattering geometry, take the following form:

$$\begin{aligned}\left\langle \frac{dN_{\text{PXR}}^{(s)}}{d\Omega} \right\rangle &= \frac{e^2 \omega_B^3 T^2 L_{\text{ext}}^{(s)}}{2\pi^4 n^2} \frac{1}{\pi \psi_0^2} \int_{-\infty}^{\infty} \int_{-\infty}^{\infty} \frac{\Omega^{(s)2}}{\sigma^{(s)2}} \int_{\sqrt{\varepsilon}}^{\infty} R_{\text{PXR}}^{(s)} \\ &\times \exp \left(-\frac{\Psi_{\perp}^2 + \Psi_{\parallel}^2}{\Psi_0^2} \right) d\xi^{(s)}(\omega) d\psi_{\perp} d\psi_{\parallel},\end{aligned} \quad (7)$$

$$\begin{aligned}\left\langle \frac{dN_{\text{DTR}}^{(s)}}{d\Omega} \right\rangle &= \frac{e^2 \omega_B^3 T^2 L_{\text{ext}}^{(s)}}{2\pi^3 n^2} \varepsilon \sqrt{\varepsilon} \tanh \left(\frac{b^{(s)}}{\sqrt{\varepsilon}} \right) \frac{1}{\pi \psi_0^2} \\ &\times \int_{-\infty}^{\infty} \int_{-\infty}^{\infty} \frac{\Omega^{(s)2} \exp \left(-\frac{\Psi_{\perp}^2 + \Psi_{\parallel}^2}{\Psi_0^2} \right)}{\sigma^{(s)2} (v^{(s)} \sigma^{(s)} - 1)^2} d\psi_{\perp} d\psi_{\parallel},\end{aligned} \quad (8)$$

$$\begin{aligned}\left\langle \frac{dN_{\text{INT}}^{(s)}}{d\Omega} \right\rangle &= \frac{e^2 \omega_B^3 T^2 L_{\text{ext}}^{(s)}}{2\pi^4 n^2} \frac{1}{\pi \psi_0^2} \int_{-\infty}^{\infty} \int_{-\infty}^{\infty} \frac{\Omega^{(s)2}}{\sigma^{(s)2} (v^{(s)} \sigma^{(s)} - 1)} \\ &\times \int_{\sqrt{\varepsilon}}^{\infty} R_{\text{INT}}^{(s)} d\xi^{(s)}(\omega) \exp \left(-\frac{\Psi_{\perp}^2 + \Psi_{\parallel}^2}{\Psi_0^2} \right) d\psi_{\perp} d\psi_{\parallel},\end{aligned} \quad (9)$$

Expressions (7)–(9) make it possible to study the influence of the parameters of the target and electron beam on the PXR and DTR angular densities and their interference.

NUMERICAL CALCULATIONS

Using the obtained equations (7)–(9), the angular density of radiation can be calculated. We consider the coherent X-ray radiation of a beam of relativistic electrons crossing a target with the thickness $L = 2 \mu\text{m}$,

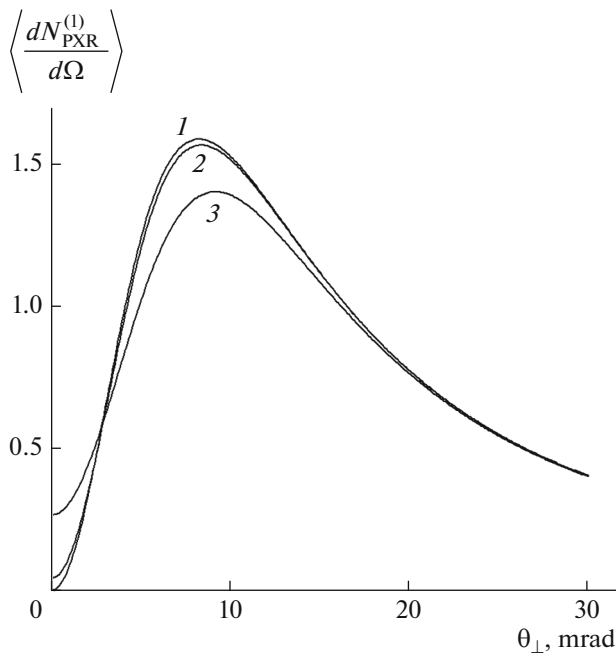


Fig. 2. Angular densities of PXR for different electron-beam divergences ψ_0 equal to (1) 0, (2) 1, and (3) 3 mrad; $\gamma = 500$, $r = \frac{l_2}{l_1} = 1$, and $L = 2 \mu\text{m}$.

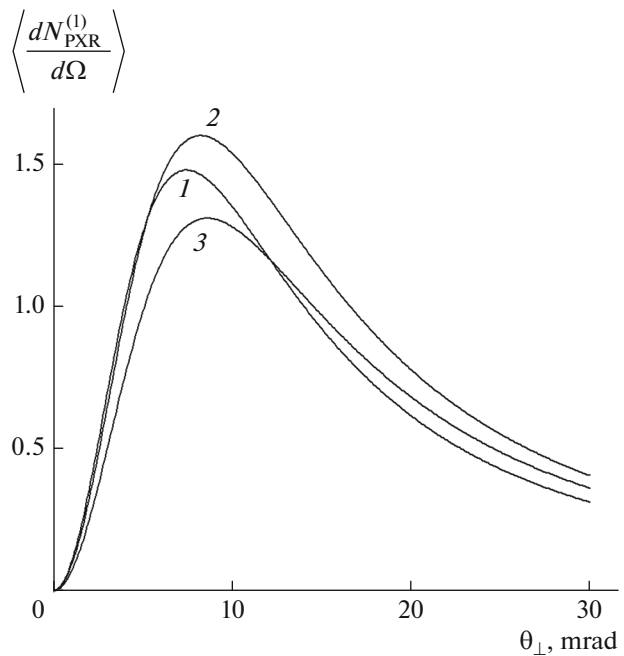


Fig. 3. Angular densities of PXR for different ratios of layer thicknesses of the periodic structure (l_2/l_1): (1) 0.5, (2) 1.0, and (3) 1.5; $\gamma = 500$, $\psi_0 = 0.1 \text{ mrad}$, and $L = 2 \mu\text{m}$.

which consists of periodically arranged layers of carbon and tungsten (C–W) with a period of $T = l_1 + l_2 = 0.002 \mu\text{m}$, for the case of symmetric reflection when the target layers are parallel to the target surface ($\delta = 0$ and $\varepsilon = 1$). If we set the angle between the relativistic-electron-beam axis and the reflecting layers (Bragg angle) as equal to $\theta_B = 2.25^\circ$, then the Bragg frequency is $\omega_B = 8 \text{ keV}$. The calculations were carried out for the case of $s = 1$ (σ -polarized waves).

Figure 2 shows the curves constructed according to formula (7), which describe the angular densities of the parametric X-ray radiation of a beam of relativistic electrons with the Lorentz factor $\gamma = 500$ for different values of the initial divergence ψ_0 of the electron beam. The size of the angular density corresponds to the number of emitted photons per electron per steradian. Figure 2 shows that the angular density depends on the divergence of the electron beam. As can be seen from Fig. 2, the angular density of PXR in a periodic layered medium under the studied conditions is more than two orders of magnitude higher than the angular density in a single crystal. This is determined by the large width of the spectral density of PXR in a periodic layered medium. Figure 3 shows the dependence of the angular density of PXR on the ratios of the layer thicknesses of the periodic structure. It follows from Fig. 3 that the angular density of PXR for constant layer period T substantially decreases with an increase

in the tungsten-layer thickness l_1 and a decrease in the carbon layer thickness l_2 .

Figure 4 shows the curves constructed by formula (8), which describe the angular density of DTR for various electron-beam divergences. Figure 4 shows a stronger dependence of the angular density of DTR on the divergence compared to the angular density of PXR. This is due to the fact that the angular density of DTR has a narrower distribution than the angular density of PXR. It follows from Figs. 2 and 4 that the angles corresponding to the maxima of the PXR and DTR density with respect to the velocity vector of a relativistic electron are approximately equal to 10 and 2 mrad, respectively. Figure 5 shows the curves describing the angular density of DTR with relativistic electrons whose energy is higher ($\gamma = 5000$) than in Fig. 4. Hence, we can conclude that the angular density of PXR substantially increases with an increase in the electron energy. At the same time, one can observe a substantial increase in the sensitivity of the angular density of DTR to changes in the angular divergence of the electron beam. As can be seen from Fig. 5, the angular densities of DTR at $\psi_0 = 0.1 \text{ mrad}$ and $\psi_0 = 0 \text{ mrad}$ are substantially different, which indicates a stronger dependence of the angular density of DTR on the electron-beam divergence with an increase in the electron energy. This is due to a substantial decrease in the emission angle corresponding to the maximum of the angular density of DTR in the range from 2 to 0.2 mrad with an increase in the electron energy. Since the angular density of DTR is uniquely related to the

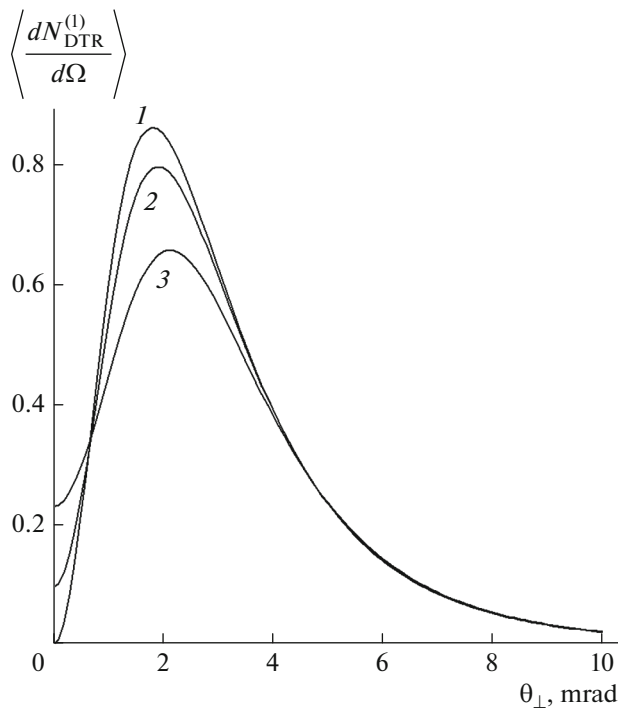


Fig. 4. Angular densities of DTR at different electron-beam divergences ψ_0 equal to (1) 0, (2) 0.5, and (3) 1.0 mrad; $\gamma = 500$, $r = \frac{l_2}{l_1} = 1$, and $L = 2 \mu\text{m}$.

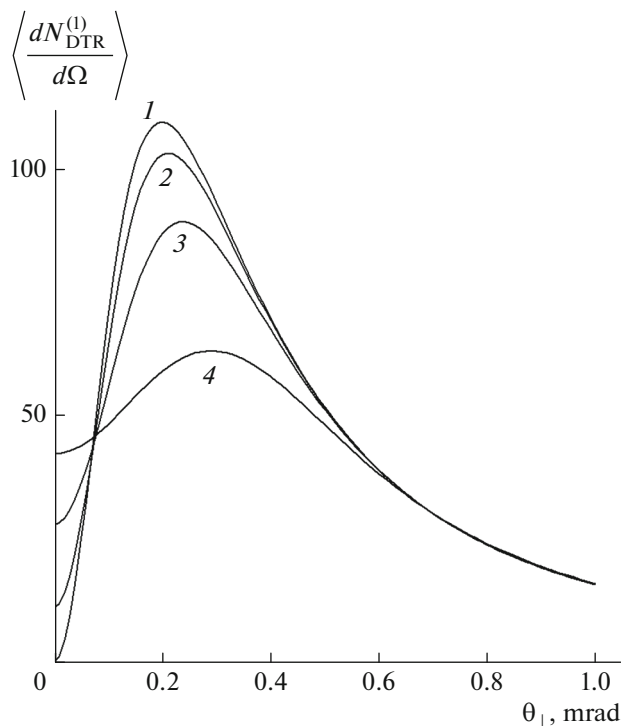


Fig. 5. Angular densities of DTR at different electron-beam divergences ψ_0 equal to (1) 0, (2) 0.05, (3) 0.10, and (4) 0.20 mrad, but with a relativistic-electron energy higher than in Fig. 4: $\gamma = 5000$, $r = \frac{l_2}{l_1} = 1$, and $L = 2 \mu\text{m}$.

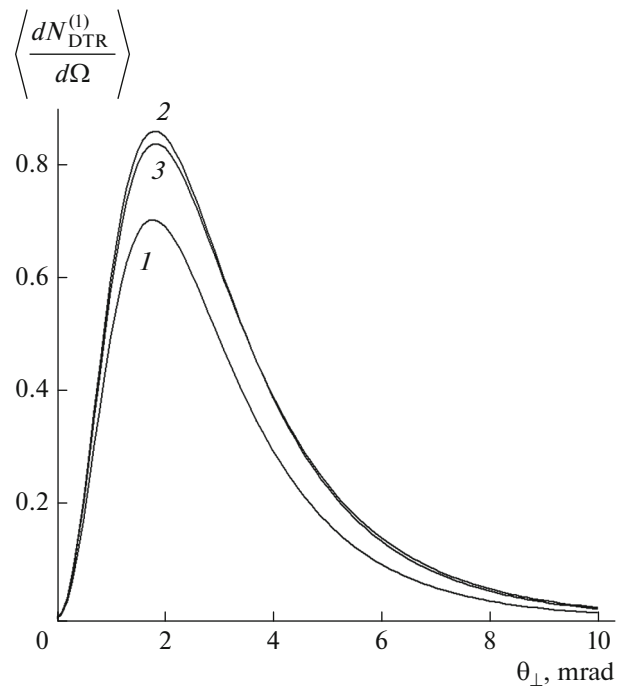


Fig. 6. Angular densities of DTR for different ratios of layer thicknesses of the periodic structure (l_2/l_1): (1) 0.5, (2) 1.0, and (3) 1.5; $\gamma = 500$, $\psi_0 = 0.1$ mrad, and $L = 2 \mu\text{m}$.

electron-beam divergence, it can be used to determine the beam divergence in various high-energy electron accelerators. Figure 6 shows the dependence of the angular density of DTR on the ratio of the target-layer thicknesses. It follows from Fig. 6 that a decrease in the thickness of the tungsten layer (and an increase in the thickness of the carbon layer) at a constant value of the period of the layered structure leads to a decrease in the angular density of DTR, in contrast to PXR (Fig. 3).

CONCLUSIONS

The parametric X-rays and diffracted transition radiation of a beam of relativistic electrons crossing a target with a periodic layered structure in the Bragg scattering geometry are studied. Expressions that describe the angular densities of the PXR, DTR, and their interference are obtained. The angular densities of radiation for various values of the parameters of the target and electron beam are numerically calculated. It is shown that the angular density of PXR depends on the electron-beam divergence. A dependence of the PXR angular density on the ratio of layer thicknesses of the periodic structure is shown, namely, the angular density of PXR at a constant value of the period of the structure noticeably decreases with an increase in the tungsten-layer thickness (and with a decrease in the carbon-layer thickness). A strong dependence of the angular density of DTR on the electron-beam

divergence is shown. It is found that the dependence of the angular density of DTR on the electron-beam divergence increases becomes stronger with an increase in the electron energy. It is shown that an increase in the thickness of the tungsten layer (and a decrease in the thickness of the carbon layer) leads to an increase in the angular density of DTR, in contrast to the angular density of PXR.

FUNDING

This work was supported by the Russian Science Foundation, project. no.19-19-00316 (extnesion) and was performed using equipment of the HghTechnology Center at the Shukhov Belgorod State Technological University.

CONFLICT OF INTEREST

The authors declare that they have no conflicts of interest.

REFERENCES

1. N. N. Nasonov, V. V. Kaplin, S. R. Uglov, M. A. Piestrup, and C. K. Gary, *Phys. Rev. E* **68**, 3604 (2003).
2. G. M. Garibyan and Ya. Shi, *Zh. Eksp. Teor. Fiz.* **61**, 930 (1971).
3. V. G. Baryshevskii and I. D. Feranchuk, *Zh. Eksp. Teor. Fiz.* **61**, 944 (1971).
4. V. G. Baryshevsky, *Nucl. Instrum. Methods Phys. Res., Sect A* **122**, 13 (1997).
5. X. Artru and P. Rullhusen, *Nucl. Instrum. Methods Phys. Res., Sect B* **145**, 1 (1998).
6. N. N. Nasonov, *Phys. Lett. A* **246**, 148 (1998).
7. V. V. Kaplin, S. R. Uglov, V. N. Zabaev, M. A. Piestrup, C. K. Gary, N. N. Nasonov, and M. K. Fuller, *Appl. Phys. Lett.* **76**, 3647 (2000).
<https://doi.org/10.1063/1.126735>
8. S. V. Blazhevich, I. V. Kolosova, and A. V. Noskov, *J. Exp. Theor. Phys.* **114**, 547 (2012).
9. S. V. Blazhevich, Yu. P. Gladkikh, A. V. Noskov, *J. Surf. Invest.: X-ray, Synchrotron Neutron Tech.* **7**, 388 (2013).
<https://doi.org/10.1134/S1027451013020080>
10. S. V. Blazhevich, A. V. Noskov, *J. Exp. Theor. Phys.* **125**, 223 (2017).
<https://doi.org/10.7868/S004445101708005369>
11. S. V. Blazhevich, N. I. Moskalenko, T. V. Kos'kova, A. V. Noskov, and E. A. Tkachenko, *J. Surf. Invest.: X-ray, Synchrotron Neutron Tech.* **11**, 49 (2017).
12. S. Blazhevich and A. Noskov, *Nucl. Instrum. Methods Phys. Res., Sect. B* **309**, 70 (2013).
13. S. V. Blazhevich and A. V. Noskov, *J. Exp. Theor. Phys.* **123**, 551 (2016).
14. S. V. Blazhevich, M. V. Bronnikova, and A. V. Noskov, *J. Surf. Invest.: X-ray, Synchrotron Neutron Tech.* **14**, 922 (2020).
15. S. V. Blazhevich, Yu. A. Drygina, O. Yu. Shevchuk, and A. V. Noskov, *J. Surf. Invest.: X-ray, Synchrotron Neutron Tech.* **14**, 586 (2020).
16. S. V. Blazhevich, M. V. Bronnikova, and A. V. Noskov, *Phys. Lett. A* **384**, 126321 (2020).
17. S. V. Blazhevich, K. S. Lyushina, and A. V. Noskov, *J. Exp. Theor. Phys.* **128**, 212 (2019).
18. S. V. Blazhevich, A. V. Noskov, *J. Exp. Theor. Phys.* **125**, 223 (2017).
19. M. V. Alyabyeva, S. V. Blazhevich, A. S. Gorlov, A. V. Noskov, and A. E. Fedoseev, *J. Surf. Invest.: X-ray, Synchrotron Neutron Tech.* **15**, 596 (2021).
20. D. O. Shkuropat, S. V. Blazhevich, A. S. Gorlov, A. V. Noskov, and A. E. Fedoseev, *J. Surf. Invest.: X-ray, Synchrotron Neutron Tech.* **15**, 717 (2021).

Translated by O. Kadkin